

# On the Convergence of the Multi-scale Deep Neural Network (MscaleDNN) in Approximating Oscillatory Functions

Bo Wang<sup>1</sup>, Heng Yuan<sup>1</sup>, Lizuo Liu<sup>2</sup>, Wenzhong Zhang<sup>3</sup>, Wei Cai<sup>2,\*</sup>

<sup>1</sup> LCSM(MOE), School of Mathematics and Statistics, Hunan Normal University, Changsha, Hunan, 410081, P. R. China.

<sup>2</sup> Dept. of Mathematics, Southern Methodist University, Dallas, TX 75275.

<sup>3</sup> Suzhou Institute for Advanced Research, University of Science and Technology of China, Suzhou, Jiangsu 215000, China.

---

**Summary.** In this paper, we derive diffusion models for the error evolution for a learning algorithm by a multiscale deep neural network (MscaleDNN) [7] in approximating oscillatory functions and solutions of boundary value problem of differential equations. The diffusion models in the spectral domain for the error of the MscaleDNN trained by a gradient descent optimization algorithm are obtained when the learning rate goes to zero and the width of network goes to infinity. The diffusion coefficients of the models possess supports covering wider range of frequency as the number of scales used in MscaleDNN increases, compared to that for a normal fully connected neural network. Numerical results of the diffusion models shows faster error decay of the MscaleDNN over a wide frequency range, thus validating the advantages of using the MscaleDNN in the approximating highly oscillated functions.

**AMS subject classifications:** 35Q68, 65N99, 68T07, 76M99

**Key words:** multi-scale neural network, convergence analysis, diffusion equation, gradient descent method.

---

## 1 Introduction

Deep neural networks (DNNs) have been actively researched as a powerful technique to approximate functions and solutions of PDEs for scientific computing applications [2, 6, 8–10]. However, recent work [13] have indicated that common fully connected DNNs demonstrated a spectral bias in learning functions with wide range of frequency information, namely, the lower frequency content of the function can be learned quickly while the convergence to higher frequency content may follow, but requiring large amount of

---

\*Corresponding author.

training for the networks. Such a phenomena differs from the behavior of the convergence of traditional multigrid methods for finding approximate solutions to PDEs whereas the higher frequency error is eliminated first. In order to remedy the spectral bias of the DNNs, a multiscale DNN method was proposed [7, 12], which consists of a series of parallel common fully connected sub-neural networks. Each of the sub-networks will receive a scaled version of the input and their outputs will then be combined to produce the output of the MscaleDNN (refer to Fig. 1). The individual sub-network in the MscaleDNN with a scaled input is designed to approximate a segment of frequency content of the targeted function and the effect of the scaling is to convert a specific range of high frequency content to a lower one so the learning can be accomplished much quickly. In the design of the multiscale DNN, in order to produce scale separation and identification capability of the MscaleDNN, activation functions with a localized frequency profile, compared with normal activation functions, e.g., ReLU, tanh, etc. This is similar to the idea of compact mother scaling and wavelet functions from the wavelet theory [1].

Although, the MultiscaleDNN has been used in computing oscillatory solutions of Navier-Stokes flows and PDEs [7, 12] with oscillatory solutions, there is no rigorous mathematical analysis which explains the reasons for its much improvement performance in approximating highly oscillatory functions compared with the plain fully connected DNNs. In this paper, we will use the neural tangent kernel (NTK) framework to derive a diffusion model for the dynamics of the error of the learning by MscaleDNN in the frequency domain in the limiting case where the learning rate goes to zero and the width of network goes to infinity. As more scales are used in the MscaleDNN, the diffusion coefficients of the diffusion equations for the error manifest its effect over larger frequency ranges while those for the normal fully connected DNN concentrates low frequency near zero-frequency. As a result, the derived diffusion model provides clear evidence why the MscaleDNN can learn quickly over a wider range of frequency range with more scales employed.

The rest of the paper is organized as follows. In Section 2, a brief review of the MscaleDNN is given. Section 2 derives the diffusion model of the learning error for fitting a function and finding the solution of a boundary value problem of an ODE. Numerical methods and solutions for the error diffusion equations will be presented in Section 4, which clearly shows the improved convergence of the MscaleDNN over wider range of frequencies while the number of scales used in MscaleDNN is increased. Finally, section 5 gives the conclusion and future work.

## 2 Brief review of MscaleDNN

Fig. 1 shows the schematics of a MscaleDNN consisting of  $n$  networks. Each scaled input passing through a sub-network can be expressed in the following formula

$$f_{\theta}(x) = \mathbf{W}^{[L-1]} \sigma \circ (\dots (\mathbf{W}^{[1]} \sigma \circ (\mathbf{W}^{[0]}(x) + \mathbf{b}^{[0]}) + \mathbf{b}^{[1]}) \dots) + \mathbf{b}^{[L-1]}, \quad (2.1)$$

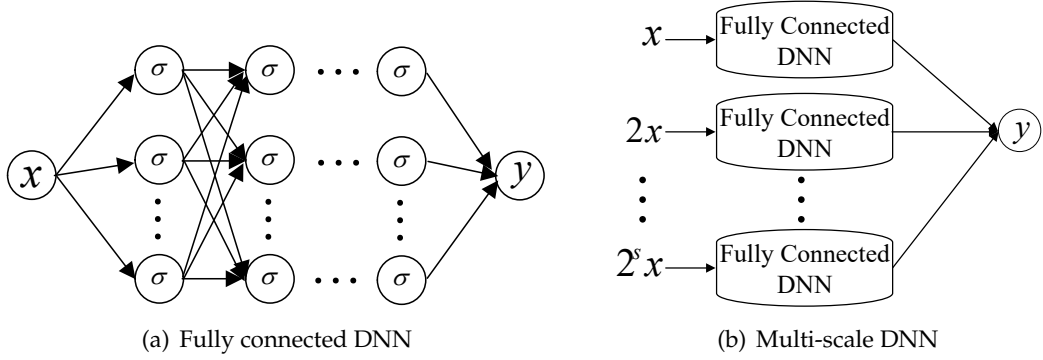


Figure 1: Illustration of fully connected DNN and Multi-scale DNN.

where  $W^{[1]}$  to  $W^{[L-1]}$  and  $b^{[1]}$  to  $b^{[L-1]}$  are the weight matrices and bias unknowns, respectively, to be optimized via the training,  $\sigma(x)$  is the activation function. In this work, the following plane wave activation function will be used for its localized frequency property [7],

$$\sigma(x) = \sin(x). \quad (2.2)$$

For the input scales, we could select the scale for the  $i$ -th sub-network to be  $i$  (as shown in Fig. 1) or  $2^{i-1}$ . Mathematically, a MscaleDNN solution  $f(x)$  is represented by the following sum of sub-networks  $f_{\theta^{n_i}}$  with network parameters denoted by  $\theta^{n_i}$  (i.e., weight matrices and bias)

$$f(x) \sim \sum_{i=1}^M f_{\theta^{n_i}}(\alpha_i x), \quad (2.3)$$

where  $\alpha_i$  is the chosen scale for the  $i$ -th sub-network in Fig. 1. For more details on the design and discussion of the MscaleDNN, please refer to [7, 12].

For comparison studies in this paper, we will refer to a “**normal**” network as an one fully connected DNN with the same total number of neurons as the MscaleDNN, but without multi-scale features. We would perform extensive numerical experiments to examine the effectiveness of different settings and select efficient ones to solve complex problems.

### 3 Error diffusion model of MscaleDNN

In this section, the convergence of machine learning algorithm for fitting and PDE approximation problems with multi-scale neural networks is analyzed. In both scenario, we show that the evolution of the error can be modeled by a diffusion equation in the Fourier frequency domain as the width of the network goes to infinity and learning rate approaches to zero.

### 3.1 Error analysis in high dimensional fitting problem

We first consider a fitting problem with objective function  $y = f(\mathbf{x})$  defined in the  $d$ -dimensional domain  $\Omega = [-1, 1]^d \subset \mathbb{R}^d$  by a neural network. The mean square loss

$$L(\boldsymbol{\theta}) = \int_{\Omega} |\mathcal{N}(\mathbf{x}, \boldsymbol{\theta}) - f(\mathbf{x})|^2 d\mathbf{x}, \quad (3.1)$$

for a neural network function  $\mathcal{N}(\mathbf{x}, \boldsymbol{\theta})$  is adopted in the following analysis.

The gradient descent dynamics based on the corresponding loss functional (3.1) is

$$\boldsymbol{\theta}^{(k+1)} = \boldsymbol{\theta}^{(k)} - \tau \nabla L(\boldsymbol{\theta}^{(k)}), \quad (3.2)$$

where  $\tau$  is the learning rate. By regarding  $\tau$  as the time step size, the continuum limit dynamics for  $\tau \rightarrow 0$  is

$$\frac{d\boldsymbol{\theta}(t)}{dt} = -\nabla L(\boldsymbol{\theta}(t)). \quad (3.3)$$

With the mean square loss function (3.1), we obtain

$$\begin{aligned} \partial_t \mathcal{N}(\mathbf{x}, \boldsymbol{\theta}) &= [\nabla_{\boldsymbol{\theta}} \mathcal{N}(\mathbf{x}, \boldsymbol{\theta})]^T \frac{d\boldsymbol{\theta}}{dt} = - \int_{\Omega} (\nabla_{\boldsymbol{\theta}} \mathcal{N}(\mathbf{x}, \boldsymbol{\theta}))^T \nabla_{\boldsymbol{\theta}} \mathcal{N}(\mathbf{x}', \boldsymbol{\theta}) (\mathcal{N}(\mathbf{x}', \boldsymbol{\theta}) - f(\mathbf{x}')) d\mathbf{x}' \\ &:= - \int_{\Omega} \Theta(\mathbf{x}, \mathbf{x}'; \boldsymbol{\theta}) (\mathcal{N}(\mathbf{x}', \boldsymbol{\theta}) - f(\mathbf{x}')) d\mathbf{x}', \end{aligned} \quad (3.4)$$

for the dynamics of the network function  $\mathcal{N}(\mathbf{x}, \boldsymbol{\theta})$ , where

$$\Theta(\mathbf{x}, \mathbf{x}'; \boldsymbol{\theta}) = (\nabla_{\boldsymbol{\theta}} \mathcal{N}(\mathbf{x}, \boldsymbol{\theta}))^T \nabla_{\boldsymbol{\theta}} \mathcal{N}(\mathbf{x}', \boldsymbol{\theta}), \quad (3.5)$$

is the neural tangent kernel (NTK) [4].

A multi-scale neural network with one hidden layer (see. Fig. 2) is defined by

$$\mathcal{N}_s(\mathbf{x}, \boldsymbol{\theta}) = \frac{1}{\sqrt{m}} \sum_{p=0}^s \sum_{k=1}^q \sigma(\boldsymbol{\theta}_{pq+k}^T 2^p \mathbf{x} + b_{pq+k}), \quad \mathbf{x} \in \Omega := [-1, 1]^d, \quad (3.6)$$

where  $s+1$  is the number of scales,  $q$  is the number of neurons for each scale,  $m = (s+1)q$  is the total number of neurons in the hidden layer. Apparently, the network reduce to fully connected neural network with one hidden layer if  $s=0$  (see Fig. 3). For this simple multi-scale neural network, direct calculation gives its NTK

$$\Theta_s(\mathbf{x}, \mathbf{x}'; \boldsymbol{\theta}) = \frac{1}{m} \sum_{p=0}^s (4^p \mathbf{x}^T \mathbf{x}' + 1) \sum_{k=1}^q \sigma'(\boldsymbol{\theta}_{pq+k}^T 2^p \mathbf{x} + b_{pq+k}) \sigma'(\boldsymbol{\theta}_{pq+k}^T 2^p \mathbf{x}' + b_{pq+k}). \quad (3.7)$$

Set the activation function  $\sigma(x) = \sin(x)$  and assume all the parameters  $\{\theta_{p,k}\}$  in  $\boldsymbol{\theta}_p = (\theta_{p,1}, \theta_{p,2}, \dots, \theta_{p,d})^T$ ,  $\{b_p\}$  are independent random variables of normal distribution. Then, by the law of large numbers and identity

$$\int_{-\infty}^{\infty} \cos(x\theta + y) e^{-\frac{\theta^2}{2}} d\theta = \sqrt{2\pi} e^{-\frac{y^2}{2}} \cos y,$$

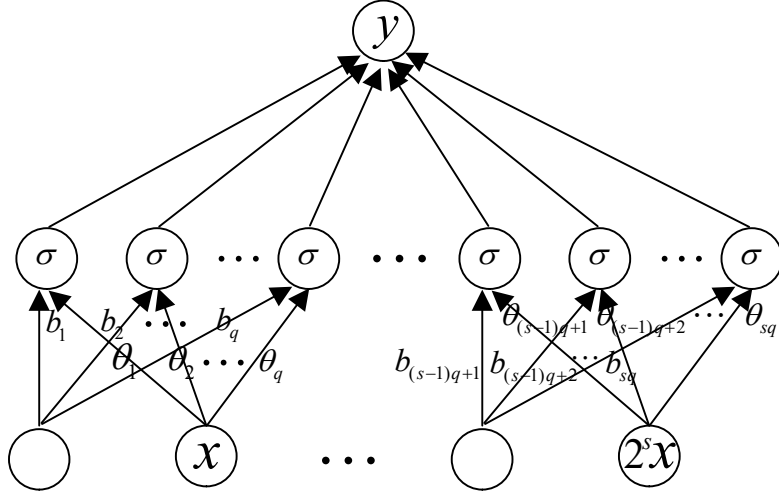


Figure 2: An illustration of an one layer multiscale DNN.

we have

$$\begin{aligned}
\lim_{q \rightarrow \infty} \Theta_s(\mathbf{x}, \mathbf{x}'; \boldsymbol{\theta}) &= \lim_{q \rightarrow \infty} \frac{1}{m} \sum_{p=0}^s (4^p \mathbf{x} \mathbf{x}' + 1) \sum_{k=1}^q \cos(\boldsymbol{\theta}_{pq+k}^T 2^p \mathbf{x} + b_{pq+k}) \cos(\boldsymbol{\theta}_{pq+k}^T 2^p \mathbf{x}' + b_{pq+k}) \\
&= \frac{1}{s+1} \sum_{p=0}^s (4^p \mathbf{x} \mathbf{x}' + 1) \mathbb{E}(\cos(\boldsymbol{\theta}_0^T 2^p \mathbf{x} + b_0) \cos(\boldsymbol{\theta}_0^T 2^p \mathbf{x}' + b_0)) \\
&= \frac{1}{2(s+1)} \sum_{p=0}^s (4^p \mathbf{x} \mathbf{x}' + 1) \left[ e^{-2} e^{-\frac{4^p |\mathbf{x} + \mathbf{x}'|^2}{2}} + e^{-\frac{4^p |\mathbf{x} - \mathbf{x}'|^2}{2}} \right].
\end{aligned}$$

As the width of the network goes to infinity, the dynamics of the gradient descent learning (3.4) tends to

$$\begin{aligned}
&\partial_t (\mathcal{N}_s(\mathbf{x}, \boldsymbol{\theta}) - f(\mathbf{x})) \\
&= -\frac{\mathbf{x}^T}{2(s+1)} \sum_{p=0}^s 4^p \int_{\Omega} \left[ e^{-2} \mathcal{G}_p(\mathbf{x} + \mathbf{x}') + \mathcal{G}_p(\mathbf{x} - \mathbf{x}') \right] \mathbf{x}' (\mathcal{N}_s(\mathbf{x}', \boldsymbol{\theta}) - f(\mathbf{x}')) d\mathbf{x}' \\
&\quad - \frac{1}{2(s+1)} \sum_{p=0}^s \int_{\Omega} \left[ e^{-2} \mathcal{G}_p(\mathbf{x} + \mathbf{x}') + \mathcal{G}_p(\mathbf{x} - \mathbf{x}') \right] (\mathcal{N}_s(\mathbf{x}', \boldsymbol{\theta}) - f(\mathbf{x}')) d\mathbf{x}',
\end{aligned} \tag{3.8}$$

where

$$\mathcal{G}_p(\mathbf{x}) := e^{-4^p |\mathbf{x}|^2 / 2}, \quad \mathbf{x} \in \mathbb{R}^d, \tag{3.9}$$

is the scaled Gaussian function. Define zero extension of the error function by

$$\eta(\mathbf{x}, \boldsymbol{\theta}) = \begin{cases} 0, & \mathbf{x} \notin \Omega, \\ \mathcal{N}_s(\mathbf{x}, \boldsymbol{\theta}) - f(\mathbf{x}), & \mathbf{x} \in \Omega. \end{cases} \tag{3.10}$$

Then, the dynamic system (3.8) can be rewritten as

$$\begin{aligned} \partial_t \eta(\mathbf{x}, \boldsymbol{\theta}) &= -\frac{\mathbf{x}^\top}{2(s+1)} \sum_{p=0}^s 4^p \int_{\mathbb{R}^d} \left[ e^{-2} \mathcal{G}_p(\mathbf{x} + \mathbf{x}') + \mathcal{G}_p(\mathbf{x} - \mathbf{x}') \right] \mathbf{x}' \eta(\mathbf{x}', \boldsymbol{\theta}) d\mathbf{x}' \\ &\quad - \frac{1}{2(s+1)} \sum_{p=0}^s \int_{\mathbb{R}^d} \left[ e^{-2} \mathcal{G}_p(\mathbf{x} + \mathbf{x}') + \mathcal{G}_p(\mathbf{x} - \mathbf{x}') \right] \eta(\mathbf{x}', \boldsymbol{\theta}) d\mathbf{x}'. \end{aligned} \quad (3.11)$$

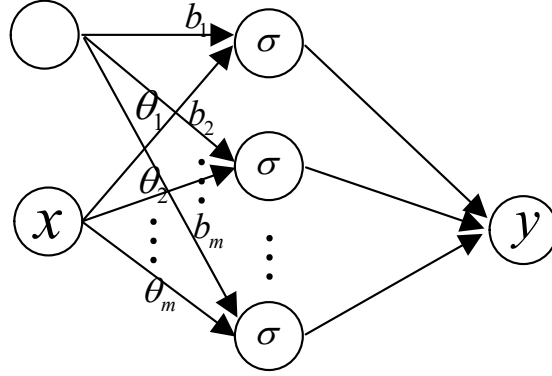


Figure 3: An illustration of an one layer fully connected DNN.

Given any  $g(\mathbf{x}) \in L^1(\mathbb{R}^d)$ , define its Fourier transform

$$\hat{g}(\boldsymbol{\xi}) := \mathcal{F}[g](\boldsymbol{\xi}) = \int_{\mathbb{R}^d} g(\mathbf{x}) e^{-i2\pi\boldsymbol{\xi}^\top \mathbf{x}} d\mathbf{x}. \quad (3.12)$$

Then, we have identities

$$\mathcal{F}[\nabla g](\boldsymbol{\xi}) = 2\pi i \boldsymbol{\xi} \mathcal{F}[g](\boldsymbol{\xi}), \quad \nabla \hat{g}(\boldsymbol{\xi}) = -2\pi i \mathcal{F}[xg(\mathbf{x})](\boldsymbol{\xi}), \quad \forall xg(\mathbf{x}) \in (L^1(\mathbb{R}^d))^d, \quad (3.13)$$

and

$$\mathcal{F}[e^{-|\mathbf{x}|^2}](\boldsymbol{\xi}) = \pi^{\frac{d}{2}} e^{-\pi^2 |\boldsymbol{\xi}|^2}, \quad \mathcal{F}[g(a\mathbf{x})](\boldsymbol{\xi}) = \left(\frac{1}{|a|}\right)^d \mathcal{F}[g]\left(\frac{\boldsymbol{\xi}}{a}\right). \quad (3.14)$$

Given any functions  $h(\mathbf{x}), g(\mathbf{x})$ , their cross-correlation and convolution are given by

$$h \star g := \int_{\mathbb{R}^d} \overline{h(\mathbf{x}')} g(\mathbf{x} + \mathbf{x}') d\mathbf{x}', \quad h * g := \int_{\mathbb{R}^d} h(\mathbf{x}') g(\mathbf{x} - \mathbf{x}') d\mathbf{x}', \quad (3.15)$$

Then, there holds the identities

$$\widehat{h \star g}(\boldsymbol{\xi}) = \widehat{h}(\boldsymbol{\xi}) \widehat{g}(\boldsymbol{\xi}), \quad \widehat{h * g}(\boldsymbol{\xi}) = \widehat{h}(\boldsymbol{\xi}) \widehat{g}(\boldsymbol{\xi}). \quad (3.16)$$

Taking Fourier transform (3.12) on both sides of (3.11) with respect to  $\mathbf{x}$  and then applying (3.13)-(3.16) to rearrange the terms gives partial differential equation

$$\begin{aligned} \frac{\partial \hat{\eta}(\boldsymbol{\xi}, \boldsymbol{\theta}(t))}{\partial t} &= \frac{1}{8\pi^2(s+1)} \nabla_{\boldsymbol{\xi}} \cdot \left[ \sum_{p=0}^s 4^p \hat{\mathcal{G}}_p(\boldsymbol{\xi}) \left( \nabla_{\boldsymbol{\xi}} \hat{\eta}(\boldsymbol{\xi}, \boldsymbol{\theta}(t)) - e^{-2} \nabla_{\boldsymbol{\xi}} \overline{\hat{\eta}(\boldsymbol{\xi}, \boldsymbol{\theta}(t))} \right) \right] \\ &\quad - \frac{1}{2(s+1)} \sum_{p=0}^s \hat{\mathcal{G}}_p(\boldsymbol{\xi}) [e^{-2} \bar{\eta}(\boldsymbol{\xi}, \boldsymbol{\theta}(t)) + \hat{\eta}(\boldsymbol{\xi}, \boldsymbol{\theta}(t))]. \end{aligned} \quad (3.17)$$

where

$$\hat{\mathcal{G}}_p(\boldsymbol{\xi}) = (2\pi)^{\frac{d}{2}} 2^{-pd} e^{-\frac{2\pi^2 |\boldsymbol{\xi}|^2}{4^p}} \quad (3.18)$$

Define

$$A_s^{\pm}(\boldsymbol{\xi}) = \frac{1 \pm e^{-2}}{8\pi^2(s+1)} \sum_{p=0}^s 4^p \hat{\mathcal{G}}_p(\boldsymbol{\xi}), \quad B_s^{\pm}(\boldsymbol{\xi}) = \frac{1 \pm e^{-2}}{2(s+1)} \sum_{p=0}^s \hat{\mathcal{G}}_p(\boldsymbol{\xi}), \quad (3.19)$$

and denote  $\hat{\eta}(\boldsymbol{\xi}, \boldsymbol{\theta}(t)) = \hat{\eta}_{\text{re}}(\boldsymbol{\xi}, \boldsymbol{\theta}(t)) + i\hat{\eta}_{\text{im}}(\boldsymbol{\xi}, \boldsymbol{\theta}(t))$ . The diffusion equation (3.17) can be rewritten as two independent equations

$$\begin{aligned} \frac{\partial \hat{\eta}_{\text{re}}(\boldsymbol{\xi}, \boldsymbol{\theta}(t))}{\partial t} &= \nabla_{\boldsymbol{\xi}} \cdot \left[ A_s^-(\boldsymbol{\xi}) \nabla_{\boldsymbol{\xi}} \hat{\eta}_{\text{re}}(\boldsymbol{\xi}, \boldsymbol{\theta}(t)) \right] - B_s^+(\boldsymbol{\xi}) \hat{\eta}_{\text{re}}(\boldsymbol{\xi}, \boldsymbol{\theta}(t)), \\ \frac{\partial \hat{\eta}_{\text{im}}(\boldsymbol{\xi}, \boldsymbol{\theta}(t))}{\partial t} &= \nabla_{\boldsymbol{\xi}} \cdot \left[ A_s^+(\boldsymbol{\xi}) \nabla_{\boldsymbol{\xi}} \hat{\eta}_{\text{im}}(\boldsymbol{\xi}, \boldsymbol{\theta}(t)) \right] - B_s^-(\boldsymbol{\xi}) \hat{\eta}_{\text{im}}(\boldsymbol{\xi}, \boldsymbol{\theta}(t)). \end{aligned} \quad (3.20)$$

with respect to the real and imaginary parts of  $\hat{\eta}(\boldsymbol{\xi}, \boldsymbol{\theta}(t))$ .

A simpler diffusion equation can be derived if the bias are set to zero in the network. In fact, a function represented by the network without bias has the form

$$\mathcal{N}_s(\mathbf{x}, \boldsymbol{\theta}) = \frac{1}{\sqrt{m}} \sum_{p=0}^s \sum_{k=1}^q \sigma(\boldsymbol{\theta}_{pq+k}^{\text{T}} 2^p \mathbf{x}), \quad \mathbf{x} \in \Omega := [-1, 1]^d, \quad (3.21)$$

and the neural tangent kernel is given by

$$\Theta_s(\mathbf{x}, \mathbf{x}'; \boldsymbol{\theta}) = \frac{\mathbf{x}^{\text{T}} \mathbf{x}'}{m} \sum_{p=0}^s 4^p \sum_{k=1}^q \sigma'(\boldsymbol{\theta}_{pq+k}^{\text{T}} 2^p \mathbf{x}) \sigma'(\boldsymbol{\theta}_{pq+k}^{\text{T}} 2^p \mathbf{x}'). \quad (3.22)$$

Set the activation function  $\sigma(x) = \sin(x)$ , and assume all the parameters  $\{\theta_p\}$  are independent random variables of normal distribution. Then, by law of large numbers, we have

$$\begin{aligned} \lim_{q \rightarrow \infty} \Theta_s(\mathbf{x}, \mathbf{x}'; \boldsymbol{\theta}) &= \lim_{q \rightarrow \infty} \frac{\mathbf{x}^{\text{T}} \mathbf{x}'}{m} \sum_{p=0}^s 4^p \sum_{k=1}^q \cos(\boldsymbol{\theta}_{pq+k}^{\text{T}} 2^p \mathbf{x}) \cos(\boldsymbol{\theta}_{pq+k}^{\text{T}} 2^p \mathbf{x}') \\ &= \frac{\mathbf{x}^{\text{T}} \mathbf{x}'}{2(s+1)} \sum_{p=0}^s 4^p \mathbb{E}(\cos(\boldsymbol{\theta}_0^{\text{T}} 2^p \mathbf{x}) \cos(\boldsymbol{\theta}_0^{\text{T}} 2^p \mathbf{x}')) \\ &= \frac{\mathbf{x}^{\text{T}} \mathbf{x}'}{2(s+1)} \sum_{p=0}^s 4^p \left[ \mathcal{G}_p(\mathbf{x} + \mathbf{x}') + \mathcal{G}_p(\mathbf{x} - \mathbf{x}') \right]. \end{aligned} \quad (3.23)$$

As the width of the network goes to infinity, the dynamics of the gradient descent learning tends to

$$\partial_t \eta(\mathbf{x}, \theta) = -\frac{\mathbf{x}^\top}{2(s+1)} \int_{\Omega} \sum_{p=0}^s 4^p \left[ \mathcal{G}_p(\mathbf{x} + \mathbf{x}') + \mathcal{G}_p(\mathbf{x} - \mathbf{x}') \right] \mathbf{x}' \eta(\mathbf{x}', \theta) d\mathbf{x}'. \quad (3.24)$$

Mimic the derivation for (3.17), we obtain from (3.24) that

$$\begin{aligned} \frac{\partial \hat{\eta}(\boldsymbol{\xi}, \boldsymbol{\theta}(t))}{\partial t} &= \frac{1}{8\pi^2(s+1)} \nabla_{\boldsymbol{\xi}} \cdot \left[ \sum_{p=0}^s 4^p \hat{\mathcal{G}}_p(\boldsymbol{\xi}) \left( \nabla_{\boldsymbol{\xi}} \hat{\eta}(\boldsymbol{\xi}, \boldsymbol{\theta}(t)) - \nabla_{\boldsymbol{\xi}} \overline{\hat{\eta}(\boldsymbol{\xi}, \boldsymbol{\theta}(t))} \right) \right] \\ &= \frac{\mathbf{i}}{4\pi^2(s+1)} \nabla_{\boldsymbol{\xi}} \cdot \left[ \sum_{p=0}^s 4^p \hat{\mathcal{G}}_p(\boldsymbol{\xi}) \nabla_{\boldsymbol{\xi}} \hat{\eta}_{\text{im}}(\boldsymbol{\xi}, \boldsymbol{\theta}(t)) \right], \end{aligned} \quad (3.25)$$

where  $\hat{\eta}_{\text{im}}(\boldsymbol{\xi}, \boldsymbol{\theta}(t)) := \Im \left\{ \hat{\eta}(\boldsymbol{\xi}, \boldsymbol{\theta}(t)) \right\}$ . The dynamic system (3.24) in the Fourier frequency domain implies that only the imaginary part of the error evolves during the gradient descent training if a one layer multi-scale neural network without bias and activation function  $\sigma(x) = \sin(x)$  is used. This conclusion is consistent with the fact that the network function (3.21) can only be used to fit odd functions.

### 3.2 Error analysis for the approximation of differential equation

It is well known that linear differential equations are equivalent to fitting problems in the Fourier spectral domain. Here, we consider the machine learning algorithm for the two points boundary value problem:

$$\begin{cases} -v''(x) = f(x), & -1 < x < 1, \\ v(-1) = a, & v(1) = b. \end{cases} \quad (3.26)$$

The mean square loss

$$L(\boldsymbol{\theta}) = \int_{-1}^1 |\partial_{xx} w(x; \boldsymbol{\theta}) + f(x)|^2 dx = \int_{-1}^1 |\partial_{xx} w(x; \boldsymbol{\theta}) - v''(x)|^2 dx, \quad (3.27)$$

is adopted in the following analysis. In order to impose the Dirichlet boundary condition, we take the approximate function

$$w(x, \boldsymbol{\theta}) = \mathcal{N}(x, \boldsymbol{\theta}) + [a - \mathcal{N}(-1, \boldsymbol{\theta})] \frac{1-x}{2} + [b - \mathcal{N}(1, \boldsymbol{\theta})] \frac{1+x}{2}, \quad (3.28)$$

to be a modification of the neural network function  $\mathcal{N}(x; \boldsymbol{\theta})$ . Apparently, we have

$$\partial_{xx} w(x, \boldsymbol{\theta}) - v''(x) = \partial_{xx} \mathcal{N}(x, \boldsymbol{\theta}) - v''(x). \quad (3.29)$$



The gradient descent dynamics for loss functional  $L(\boldsymbol{\theta})$  is given by (3.2) and its continuum limit for  $\tau \rightarrow 0$  is given by (3.3). From (3.3), (3.27) and (3.29), we can calculate that

$$\begin{aligned} \partial_t(\mathcal{N}(x; \boldsymbol{\theta}(t)) - v(x)) &= -\nabla_{\boldsymbol{\theta}} \mathcal{N}(x; \boldsymbol{\theta}(t)) \nabla L(\boldsymbol{\theta}(t)) \\ &= -\int_{-1}^1 \partial_{x'x'} \Theta(x, x', \boldsymbol{\theta}(t)) \partial_{x'x'} (\mathcal{N}(x'; \boldsymbol{\theta}(t)) - v(x')) dx', \end{aligned} \quad (3.30)$$

where  $\Theta(x, x', \boldsymbol{\theta}(t))$  is the NTK.

Suppose the multi-scale neural network sketched in Fig. 2 is adopted, i.e.,

$$\mathcal{N}_s(x, \boldsymbol{\theta}) = \frac{1}{\sqrt{m}} \sum_{p=0}^s \sum_{k=1}^q \sigma(\theta_{pq+k} 2^p x + b_{pq+k}), \quad x \in [-1, 1], \quad (3.31)$$

which is the 1-dimensional special case of (3.6). According to (3.7), the neural tangent kernel for this 1-dimensional neural network is given by

$$\Theta_s(x, x'; \boldsymbol{\theta}) = \frac{1}{m} \sum_{p=0}^s (4^p x x' + 1) \sum_{k=1}^q \sigma'(\theta_{pq+k} 2^p x + b_{pq+k}) \sigma'(\theta_{pq+k} 2^p x' + b_{pq+k}), \quad (3.32)$$

for all  $x, x' \in [-1, 1]$ . Set the activation function  $\sigma(x) = \sin(x)$  and assume all the parameters  $\{\theta_p\}, \{b_p\}$  are independent random variables of normal distribution. Let the width of each sub neural network in the MsNN goes to infinity, we obtain

$$\Theta_s^\infty(x, x'; \boldsymbol{\theta}) := \lim_{q \rightarrow \infty} \Theta_s(x, x'; \boldsymbol{\theta}) = \frac{1}{2(s+1)} \sum_{p=0}^s (4^p x x' + 1) \left[ e^{-2} \mathcal{G}_p(x+x') - \mathcal{G}_p(x-x') \right].$$

Here,  $\mathcal{G}_p(x)$  is just the one dimension special case of the multi-dimensional Gaussian defined in (3.9). Denote zero extension of the error function by

$$\eta(x, \boldsymbol{\theta}(t)) = \begin{cases} 0, & |x| > 1, \\ \mathcal{N}_s(x, \boldsymbol{\theta}(t)) - v(x), & |x| \leq 1, \end{cases} \quad (3.33)$$

Then, the dynamics (3.30) tends to

$$\partial_t \eta(x; \boldsymbol{\theta}(t)) = -\int_{-\infty}^{+\infty} \partial_{x'x'} \Theta_s^\infty(x, x') \partial_{x'x'} \eta(x', \boldsymbol{\theta}(t)) dx', \quad (3.34)$$

as the width of the neural network goes to infinity. Note that

$$\begin{aligned} \partial_{x'x'} \Theta_s^\infty(x, x', \boldsymbol{\theta}) &= \frac{x}{s+1} \sum_{p=0}^s 4^p \left[ e^{-2} \mathcal{G}'_p(x+x') - \mathcal{G}'_p(x-x') \right] \\ &\quad + \frac{1}{2(s+1)} \sum_{p=0}^s (4^p x x' + 1) \left[ e^{-2} \mathcal{G}''_p(x+x') + \mathcal{G}''_p(x-x') \right]. \end{aligned} \quad (3.35)$$

Substituting (3.35) into (3.34) and taking 1-dimensional Fourier transform (3.12) on both sides and then applying the 1-dimensional version of (3.13)-(3.16) to rearrange the terms gives partial differential equation

$$\begin{aligned}
\partial_t \hat{\eta}(\xi, \theta(t)) &= \partial_\xi \left[ \frac{1}{2(s+1)} \sum_{p=0}^s 4^p \hat{\mathcal{G}}_p(\xi) \xi^2 \partial_\xi \left( e^{-2\overline{\partial_{xx}\eta}(\xi, \theta)} - \widehat{\partial_{xx}\eta}(\xi, \theta) \right) \right] \\
&\quad + \partial_\xi \left[ \frac{1}{s+1} \sum_{p=0}^s 4^p \hat{\mathcal{G}}_p(\xi) \xi \left( e^{-2\overline{\partial_{xx}\eta}(\xi, \theta)} - \widehat{\partial_{xx}\eta}(\xi, \theta) \right) \right] \\
&\quad + \frac{2\pi^2}{s+1} \sum_{p=0}^s \hat{\mathcal{G}}_p(\xi) \xi^2 \left( e^{-2\overline{\partial_{xx}\eta}(\xi, \theta)} + \widehat{\partial_{xx}\eta}(\xi, \theta) \right) \\
&= \partial_\xi \left[ \frac{1}{2(s+1)} \sum_{p=0}^s 4^p \hat{\mathcal{G}}_p(\xi) \partial_\xi \left( e^{-2\xi^2 \overline{\partial_{xx}\eta}(\xi, \theta)} - \xi^2 \widehat{\partial_{xx}\eta}(\xi, \theta) \right) \right] \\
&\quad + \frac{2\pi^2}{s+1} \sum_{p=0}^s \hat{\mathcal{G}}_p(\xi) \xi^2 \left( e^{-2\overline{\partial_{xx}\eta}(\xi, \theta)} + \widehat{\partial_{xx}\eta}(\xi, \theta) \right),
\end{aligned} \tag{3.36}$$

where

$$\hat{\mathcal{G}}_p(\xi) = \sqrt{2\pi} 2^{-p} e^{-\frac{2\pi^2 \xi^2}{4^p}}. \tag{3.37}$$

Define coefficients

$$A_s^\pm(\xi) = \frac{1 \pm e^{-2}}{2(s+1)} \sum_{p=0}^s 4^p \hat{\mathcal{G}}_p(\xi), \quad B_s^\pm(\xi) = \frac{2\pi^2(1 \pm e^{-2})}{s+1} \sum_{p=0}^s \hat{\mathcal{G}}_p(\xi). \tag{3.38}$$

The real and imaginary parts of  $\hat{\eta}(\xi, \theta(t))$  satisfy diffusion equations

$$\begin{aligned}
\partial_t \hat{\eta}_{\text{re}}(\xi, \theta(t)) &= -\partial_\xi \left[ A_s^-(\xi) \partial_\xi \left( \xi^2 \widehat{\partial_{xx}\eta}_{\text{re}}(\xi, \theta) \right) \right] + B_s^+(\xi) \xi^2 \widehat{\partial_{xx}\eta}_{\text{re}}(\xi, \theta), \\
\partial_t \hat{\eta}_{\text{im}}(\xi, \theta(t)) &= -\partial_\xi \left[ A_s^+(\xi) \partial_\xi \left( \xi^2 \widehat{\partial_{xx}\eta}_{\text{im}}(\xi, \theta) \right) \right] + B_s^-(\xi) \xi^2 \widehat{\partial_{xx}\eta}_{\text{im}}(\xi, \theta).
\end{aligned} \tag{3.39}$$

By introducing weighted error function  $\omega(\xi, \theta(t)) = \xi^2 \widehat{\partial_{xx}\eta}(\xi, \theta(t))$ , the diffusion equation (3.39) can be rewritten as

$$\begin{aligned}
\frac{1}{4\pi^2 \xi^4} \partial_t \omega_{\text{re}}(\xi, \theta(t)) &= \partial_\xi \left[ A_s^-(\xi) \partial_\xi \omega_{\text{re}}(\xi, \theta) \right] - B_s^+(\xi) \omega_{\text{re}}(\xi, \theta), \\
\frac{1}{4\pi^2 \xi^4} \partial_t \omega_{\text{im}}(\xi, \theta(t)) &= \partial_\xi \left[ A_s^+(\xi) \partial_\xi \omega_{\text{re}}(\xi, \theta) \right] - B_s^-(\xi) \omega_{\text{re}}(\xi, \theta).
\end{aligned} \tag{3.40}$$

## 4 Numerical analysis of the diffusion equations

According to the analysis in the above subsection, the dynamics of the gradient descent learning tends to the diffusion equations (3.20) in the Fourier spectral domain as the

width of the network goes to infinity. In general, the diffusion equations for the real and imaginary parts can be written as

$$\frac{\partial u(\boldsymbol{\zeta}, t)}{\partial t} = \nabla_{\boldsymbol{\zeta}} \cdot \left[ A_s^{\mp}(\boldsymbol{\zeta}) \nabla_{\boldsymbol{\zeta}} u(\boldsymbol{\zeta}, t) \right] - B_s^{\pm}(\boldsymbol{\zeta}) u(\boldsymbol{\zeta}, t), \quad \boldsymbol{\zeta} \in \mathbb{R}^d, \quad (4.1)$$

where the functions  $A_s^{\pm}(\boldsymbol{\zeta}), B_s^{\mp}(\boldsymbol{\zeta})$  defined in (3.19) are linear combination of scaled Gaussian functions. Apparently, both  $A_s^{\pm}(\boldsymbol{\zeta}), B_s^{\mp}(\boldsymbol{\zeta})$  are positive functions in  $\mathbb{R}^d$ . Therefore, the solution of (4.1) has energy equality

$$\frac{d}{dt} \int_{\mathbb{R}^d} |u(\boldsymbol{\zeta}, t)|^2 d\boldsymbol{\zeta} = -2 \int_{\mathbb{R}^d} \left[ A_s^{\mp}(\boldsymbol{\zeta}) \left| \nabla_{\boldsymbol{\zeta}} u(\boldsymbol{\zeta}, t) \right|^2 + B_s^{\pm}(\boldsymbol{\zeta}) |u(\boldsymbol{\zeta}, t)|^2 \right] d\boldsymbol{\zeta}, \quad (4.2)$$

which implies that the solution  $u(\boldsymbol{\zeta}, t) \rightarrow 0$  for any  $\boldsymbol{\zeta} \in \mathbb{R}^d$  as  $t \rightarrow \infty$ . That means the gradient descent learning for a fitting problem with a one layer neural network is convergent suppose the learning rate is sufficiently small and the width of the neural network is sufficiently large. Apparently, the diffusion coefficients  $\{A_s^{\pm}(\boldsymbol{\zeta}), B_s^{\mp}(\boldsymbol{\zeta})\}$  plays a key role in the convergence speed. Some examples of  $\{A_s^-(\boldsymbol{\zeta}), B_s^+(\boldsymbol{\zeta})\}$  are plotted in Fig. 4. We can see that both  $A_s^-(\boldsymbol{\zeta})$  and  $B_s^+(\boldsymbol{\zeta})$  have larger support and value as the increasing of  $s$ .

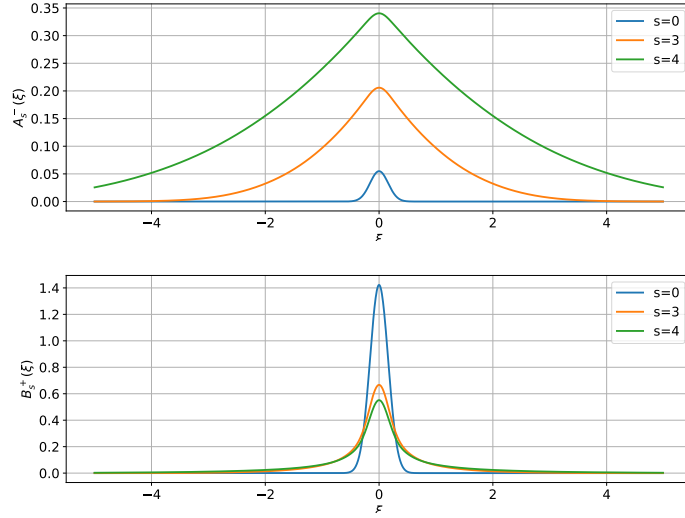


Figure 4: Diffusion coefficients  $A_s^-(\boldsymbol{\zeta})$  and  $B_s^+(\boldsymbol{\zeta})$  with  $s=0,3,4$ .

#### 4.1 Hermite spectral method for 1-dimensional case

As the analytic solutions of (4.1) are not available, we resort to numerical method to analyze the solutions of (4.1) for different numbers of scales. We will employ a Hermite spectral method for the spatial discretization of equation (4.1) due to the unbounded computational

domain and the involved Gaussian functions. For this purpose, we introduce the Hermite functions (cf. [11]) defined by

$$\hat{H}_n(x) = \frac{1}{\pi^{1/4} \sqrt{2^n n!}} e^{-x^2/2} H_n(x), \quad n \geq 0, x \in \mathbb{R}, \quad (4.3)$$

where  $H_n(x)$  are Hermite polynomials. The Hermite functions  $\hat{H}_n(x)$  are orthogonal function in  $L^2(\mathbb{R})$ , i.e.,

$$\int_{-\infty}^{\infty} \hat{H}_n(x) \hat{H}_m(x) dx = \delta_{mn}, \quad (4.4)$$

where  $\delta_{mn}$  is Kronecker symbol. We will also use the following recurrence formulas (cf. [11])

$$\begin{aligned} \hat{H}_{n+1}(x) &= x \sqrt{\frac{2}{n+1}} \hat{H}_n(x) - \sqrt{\frac{n}{n+1}} \hat{H}_{n-1}(x) = 0, \quad n \geq 1, \\ \hat{H}_0(x) &= \pi^{-1/4} e^{-x^2/2}, \quad \hat{H}_1(x) = \sqrt{2} \pi^{-1/4} x e^{-x^2/2}, \end{aligned} \quad (4.5)$$

and

$$\hat{H}'_n(x) = \sqrt{2n} \hat{H}_{n-1}(x) - x \hat{H}_n(x) = \sqrt{\frac{n}{2}} \hat{H}_{n-1}(x) - \sqrt{\frac{n+1}{2}} \hat{H}_{n+1}(x), \quad (4.6)$$

in the derivation of the Hermite spectral discretization.

We discretize the computational time interval  $[0, T]$  into equi-spaced intervals  $I_k := [k\Delta t, (k+1)\Delta t]$  for  $k=0, 1, \dots, N$ , where  $\Delta t = T/N$ . Then, the Hermite spectral method together with backward Euler time discretization is defined as: find numerical approximation

$$u_p^m(\xi) = \sum_{k=0}^p u_k^m \hat{H}_k(\lambda \xi), \quad (4.7)$$

for  $u(\xi, t)$  at time  $t_m = m\Delta t$  s.t.,

$$\left( \frac{u_p^m(\xi) - u_p^{m-1}(\xi)}{\Delta t}, \hat{H}_n(\lambda \xi) \right) = - \left( A_s^\mp(\xi) \frac{du_p^m(\xi)}{d\xi}, \frac{d\hat{H}_n(\lambda \xi)}{d\xi} \right) - (B_s^\pm(\xi) u_p^m(\xi), \hat{H}_n(\lambda \xi)), \quad (4.8)$$

for  $k=0, 1, \dots, p$ . Here,  $\lambda$  is a scaling parameter to tune the interval with effective resolution, the  $L^2$  inner product is defined as

$$(f(\xi), g(\xi)) = \int_{-\infty}^{\infty} f(\xi) g(\xi) d\xi. \quad (4.9)$$

Denoted the unknown vector by  $\mathbf{u}_p^m = (u_0^m, u_1^m, \dots, u_p^m)^\top$ , the numerical scheme (4.8) leads to linear systems

$$\mathbb{D} \frac{\mathbf{u}_p^m - \mathbf{u}_p^{m-1}}{\Delta t} = (\mathbb{K}^\mp + \mathbb{M}^\pm) \mathbf{u}_p^m, \quad (4.10)$$

where  $\mathbb{D} = (D_{nk})$ ,  $\mathbb{K}^\pm = (K_{nk}^\pm)$ ,  $\mathbb{M} = (M_{nk}^\pm)$  are matrices with entries given by

$$\begin{aligned} D_{nk} &= (\widehat{H}_k(\lambda\xi), \widehat{H}_n(\lambda\xi)) = \frac{1}{\lambda} \delta_{nk}, \quad K_{nk}^\pm = -\lambda^2 \left( A_s^\pm(\xi) \widehat{H}'_k(\lambda\xi), \widehat{H}'_n(\lambda\xi) \right), \\ M_{nk}^\pm &= -(B_s^\pm(\xi) \widehat{H}_k(\lambda\xi), \widehat{H}_n(\lambda\xi)). \end{aligned} \quad (4.11)$$

By the recurrence formula (4.5), we have

$$\begin{aligned} \widehat{H}'_k(x) \widehat{H}'_n(x) &= \left[ \sqrt{\frac{k}{2}} \widehat{H}_{k-1}(x) - \sqrt{\frac{k+1}{2}} \widehat{H}_{k+1}(x) \right] \left[ \sqrt{\frac{n}{2}} \widehat{H}_{n-1}(x) - \sqrt{\frac{n+1}{2}} \widehat{H}_{n+1}(x) \right] \\ &= \frac{\sqrt{nk}}{2} \widehat{H}_{k-1}(x) \widehat{H}_{n-1}(x) - \frac{\sqrt{(n+1)k}}{2} \widehat{H}_{k-1}(x) \widehat{H}_{n+1}(x) \\ &\quad - \frac{\sqrt{n(k+1)}}{2} \widehat{H}_{k+1}(x) \widehat{H}_{n-1}(x) + \frac{\sqrt{(n+1)(k+1)}}{2} \widehat{H}_{k+1}(x) \widehat{H}_{n+1}(x), \end{aligned} \quad (4.12)$$

for all  $n, k \geq 1$ . Therefore,

$$\begin{aligned} K_{nk}^\pm &= \frac{\sqrt{nk}}{2} C_{n-1, k-1}^\pm - \frac{\sqrt{(n+1)k}}{2} C_{n+1, k-1}^\pm \\ &\quad - \frac{\sqrt{n(k+1)}}{2} C_{n-1, k+1}^\pm + \frac{\sqrt{(n+1)(k+1)}}{2} C_{n+1, k+1}^\pm \end{aligned} \quad (4.13)$$

for all  $k \geq 1$ , where

$$C_{nk}^\pm = -\lambda^2 \int_{-\infty}^{\infty} c_s^\pm(\xi) \widehat{H}_k(\lambda\xi) \widehat{H}_n(\lambda\xi) d\xi.$$

Noting that

$$M_{nk}^\pm = - \int_{-\infty}^{\infty} d_s^\pm(\xi) \widehat{H}_k(\lambda\xi) \widehat{H}_n(\lambda\xi) d\xi, \quad (4.14)$$

and  $A_s^\pm(\xi)$ ,  $B_s^\pm(\xi)$  are linear combination of Gaussian functions as presented in (3.19), the computation of  $C_{nk}^\pm$  and  $M_{nk}^\pm$  can be reduced to compute the weighted inner products

$$I_{nk}(\tau) = \int_{-\infty}^{\infty} \widehat{H}_n(x) \widehat{H}_k(x) e^{-\tau x^2} dx = \frac{1}{\sqrt{\tau+1}} \int_{-\infty}^{\infty} \widetilde{H}_n\left(\frac{y}{\sqrt{\tau+1}}\right) \widetilde{H}_k\left(\frac{y}{\sqrt{\tau+1}}\right) e^{-y^2} dy. \quad (4.15)$$

where  $\widetilde{H}_n(x)$  is the normalized Hermite polynomial defined by  $\widetilde{H}_n(x) = e^{x^2/2} \widehat{H}_n(x)$ . In fact, for  $A_s^\pm(\xi)$ ,  $B_s^\pm(\xi)$  given in (3.19), we have

$$C_{nk}^\pm = -\frac{(1 \pm e^{-2})\lambda}{2(2\pi)^{\frac{3}{2}}(s+1)} \sum_{p=0}^s 2^p I_{nk}\left(\frac{2\pi^2}{4^p \lambda^2}\right), \quad M_{nk}^\pm = -\sqrt{\frac{\pi}{2}} \frac{1 \pm e^{-2}}{(s+1)\lambda} \sum_{p=0}^s 2^{-p} I_{nk}\left(\frac{2\pi^2}{4^p \lambda^2}\right). \quad (4.16)$$

Next, we present formulas for the calculation of the integrals  $I_{nk}(\tau)$ . Given any scaling factor  $a$ , scaled Hermite polynomial  $\widetilde{H}_n(ay)$  has formulation

$$\widetilde{H}_n(ay) = \sum_{k=0}^n h_{n,k}(a) \widetilde{H}_k(y), \quad (4.17)$$

where the coefficients  $\{h_{n,k}(a)\}$  can be calculated via recurrence formulas (4.23). Therefore,

$$\begin{aligned}
I_{nk}(\tau) &= \frac{1}{\sqrt{\tau+1}} \int_{-\infty}^{\infty} \tilde{H}_n\left(\frac{y}{\sqrt{\tau+1}}\right) \tilde{H}_k\left(\frac{y}{\sqrt{\tau+1}}\right) e^{-y^2} dy \\
&= \frac{1}{\sqrt{\tau+1}} \sum_{i=0}^n \sum_{j=0}^k h_{n,i}\left(\frac{1}{\sqrt{\tau+1}}\right) h_{k,j}\left(\frac{1}{\sqrt{\tau+1}}\right) \int_{-\infty}^{\infty} \tilde{H}_i(y) \tilde{H}_j(y) e^{-y^2} dy \\
&= \frac{1}{\sqrt{\tau+1}} \sum_{i=0}^{\min\{n,k\}} h_{n,i}\left(\frac{1}{\sqrt{\tau+1}}\right) h_{k,i}\left(\frac{1}{\sqrt{\tau+1}}\right).
\end{aligned} \tag{4.18}$$

In order to derive recurrence formulas for the coefficients  $\{h_{n,k}(a)\}$ , we recall the recurrence formula (4.5) to obtain

$$\sqrt{2(n+1)} \tilde{H}_{n+1}(ay) = 2ay \tilde{H}_n(ay) - \sqrt{2n} \tilde{H}_{n-1}(ay), \quad n \geq 1. \tag{4.19}$$

Substituting the expansion (4.17) into (4.19) gives

$$\sqrt{2(n+1)} \sum_{k=0}^{n+1} h_{n+1,k}(a) \tilde{H}_k(y) = 2ay \sum_{k=0}^n h_{n,k}(a) \tilde{H}_k(y) - \sqrt{2n} \sum_{k=0}^{n-1} h_{n-1,k}(a) \tilde{H}_k(y), \tag{4.20}$$

for  $n \geq 1$ . Noting that

$$\tilde{H}_1(y) = \sqrt{2y} \tilde{H}_0(y), \quad 2y \tilde{H}_k(y) = \sqrt{2(k+1)} \tilde{H}_{k+1}(y) + \sqrt{2k} \tilde{H}_{k-1}(y), \quad k \geq 1, \tag{4.21}$$

direct calculation gives

$$\begin{aligned}
2ay \sum_{k=0}^n h_{n,k}(a) \tilde{H}_k(y) &= a \sum_{k=1}^n h_{n,k}(a) \left[ \sqrt{2(k+1)} \tilde{H}_{k+1}(y) + \sqrt{2k} \tilde{H}_{k-1}(y) \right] + 2ay h_{n,0}(a) \tilde{H}_0(y) \\
&= a \sum_{k=0}^n \sqrt{2(k+1)} h_{n,k}(a) \tilde{H}_{k+1}(y) + a \sum_{k=1}^n \sqrt{2k} h_{n,k}(a) \tilde{H}_{k-1}(y) \\
&= a \sum_{k=1}^{n+1} \sqrt{2k} h_{n,k-1} \tilde{H}_k(y) + a \sum_{k=0}^{n-1} \sqrt{2(k+1)} h_{n,k+1} \tilde{H}_k(y).
\end{aligned}$$

Therefore, (4.20) can be rearranged into

$$\begin{aligned}
&\sqrt{2(n+1)} \sum_{k=0}^{n+1} h_{n+1,k} \tilde{H}_k(y) \\
&= a \sum_{k=1}^{n+1} \sqrt{2k} h_{n,k-1} \tilde{H}_k(y) + a \sum_{k=0}^{n-1} \sqrt{2(k+1)} h_{n,k+1} \tilde{H}_k(y) - \sqrt{2n} \sum_{k=0}^{n-1} h_{n-1,k} \tilde{H}_k(y) \\
&= [\sqrt{2a} h_{n,1} - \sqrt{2n} h_{n-1,0}] \tilde{H}_0(y) + a \sqrt{2n} h_{n,n-1} \tilde{H}_n(y) + a \sqrt{2(n+1)} h_{n,n} \tilde{H}_{n+1}(y) \\
&\quad + \sum_{k=1}^{n-1} [a \sqrt{2k} h_{n,k-1} + a \sqrt{2(k+1)} h_{n,k+1} - \sqrt{2n} h_{n-1,k}] \tilde{H}_k(y).
\end{aligned} \tag{4.22}$$

Matching the coefficients in both sides of the above equation gives us

$$\begin{aligned}
h_{n+1,0}(a) &= \sqrt{\frac{1}{n+1}} a h_{n,1}(a) - \sqrt{\frac{n}{n+1}} h_{n-1,0}(a), \\
h_{n+1,k}(a) &= a \sqrt{\frac{k}{n+1}} h_{n,k-1}(a) + a \sqrt{\frac{k+1}{n+1}} h_{n,k+1}(a) - \sqrt{\frac{n}{n+1}} h_{n-1,k}(a), \quad k=1,2,\dots,n-1, \\
h_{n+1,k}(t) &= a \sqrt{\frac{k}{n+1}} h_{n,k-1}(a), \quad k=n,n+1,
\end{aligned} \tag{4.23}$$

for all  $n \geq 1$ , while the initial values are given by

$$h_{0,0}(a) = 1, \quad h_{1,0}(a) = 0, \quad h_{1,1}(a) = a. \tag{4.24}$$

**Remark 4.1.** By induction,  $h_{n,k}(a)$  has explicit formula

$$h_{n,k}(a) = \begin{cases} 0, & n-k=2s+1, \\ \sqrt{\frac{n!}{2^{n-k} k! s!}} \frac{1}{s!} a^k (a^2-1)^s, & n-k=2s, \end{cases} \tag{4.25}$$

for all  $k=0,1,\dots,n$ .

## 4.2 Numerical results

**Example 1.** We first give a numerical example for the diffusion problem (4.1) to show the decay of the solution with respect to  $t$ . The initial function is given by

$$u(\xi,0) = \begin{cases} 1, & |x| \leq 3, \\ 0, & |x| > 3, \end{cases} \tag{4.26}$$

and three groups of diffusion coefficients  $\{A_s^\mp(\xi), B_s^\pm(\xi)\}, s=0,3,6$  are tested. For the numerical discretization of the PDE, we take  $p=100, \Delta t=1.0e-3$ . The numerical solutions at different time  $t$  are plotted in Fig. 5. The numerical results clearly show that the initial function decays faster and faster as the increasing of  $s$ . It is worthy to emphasize that diffusion coefficients  $\{A_0^\mp(\xi), B_0^\pm(\xi)\}$  only produce fast decay in a small neighborhood of the origin. These observations are consistent with the performance of the multi-scale neural network which has faster convergence especially in the approximation of highly oscillated functions.

**Example 2.** In this example, we will compare the gradient descent learning in the physical domain with the corresponding diffusion process in the Fourier spectral domain. We test a fitting problem with objective function

$$f(x) = \sin a \pi x + \cos b \pi x,$$

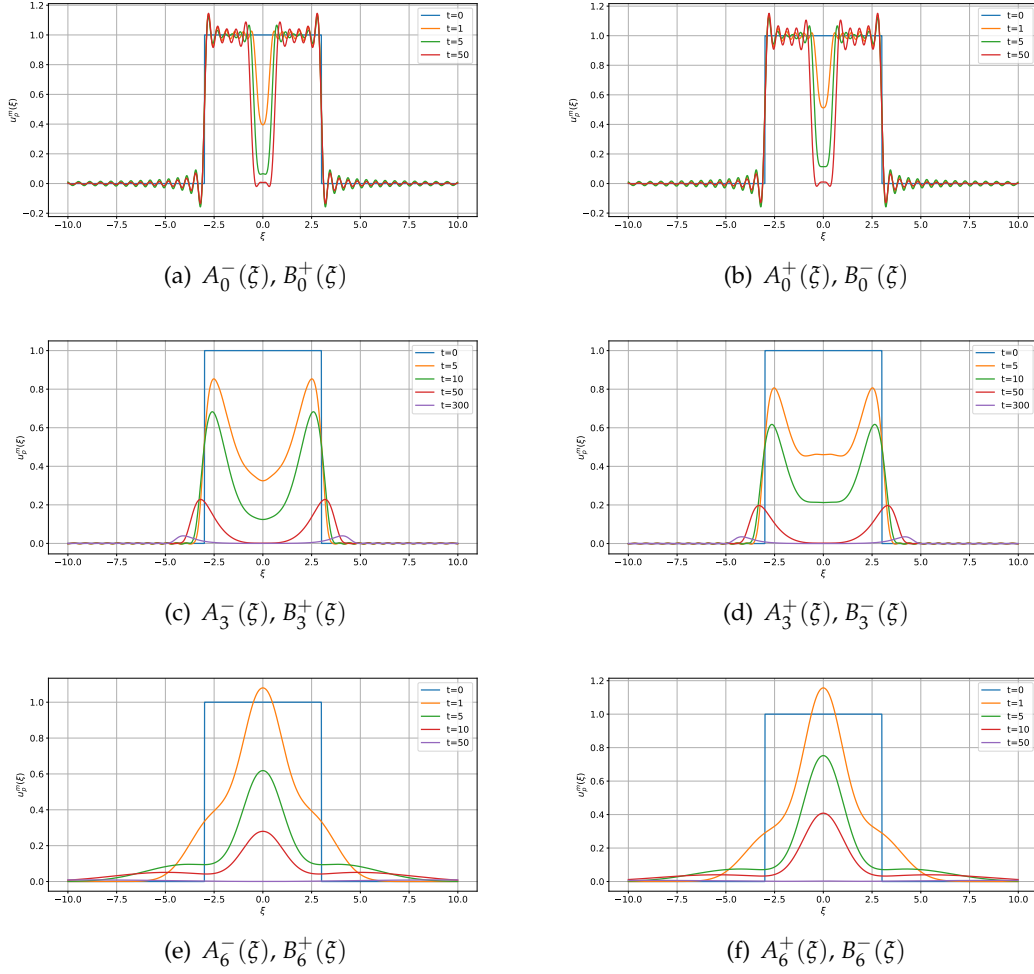


Figure 5: Numerical solution of (4.1) with three groups of diffusion coefficients.

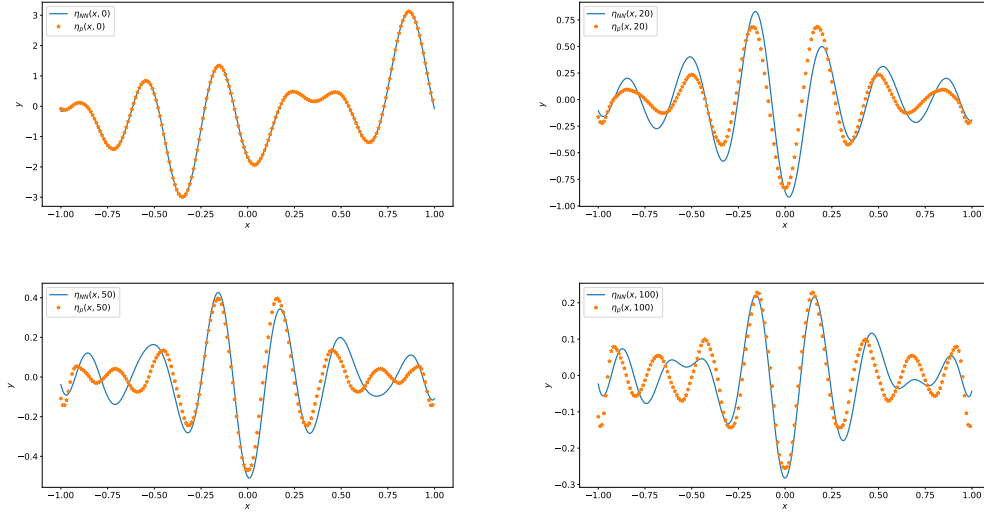
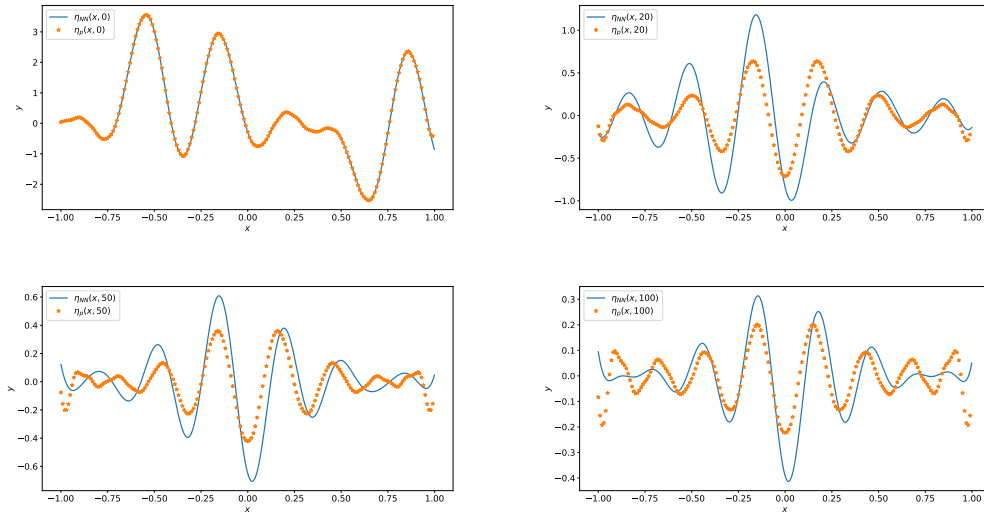
on the interval  $[-1, 1]$ . The Fourier transform of  $f(x)$  with zero extension outside  $[-1, 1]$  is

$$\hat{f}(\xi) = \frac{\sin[(b+2\xi)\pi]}{(b+2\xi)\pi} + \frac{\sin[(b-2\xi)\pi]}{(b-2\xi)\pi} + i \left[ \frac{\sin[(a+2\xi)\pi]}{(a+2\xi)\pi} - \frac{\sin[(a-2\xi)\pi]}{(a-2\xi)\pi} \right].$$

For the one layer multi-scale neural network, the Fourier transform of  $\mathcal{N}_s(x, \theta)$  we can be calculated as

$$\begin{aligned} \widehat{\mathcal{N}}_s(\xi, \theta) &= \frac{1}{\sqrt{m}} \sum_{p=0}^s \sum_{k=1}^q \frac{-2\pi i \xi (e^{2\pi i \xi} \sin(2^p \theta_{pq+k} - b_{pq+k}) + e^{-2\pi i \xi} \sin(2^p \theta_{pq+k} + b_{pq+k}))}{4^p \theta_{pq+k}^2 - 4\pi^2 \xi^2} \\ &+ \frac{1}{\sqrt{m}} \sum_{p=0}^s \sum_{k=1}^q \frac{2^p \theta_{pq+k} (e^{2\pi i \xi} \cos(2^p \theta_{pq+k} - b_{pq+k}) - e^{-2\pi i \xi} \cos(2^p \theta_{pq+k} + b_{pq+k}))}{4^p \theta_{pq+k}^2 - 4\pi^2 \xi^2}. \end{aligned}$$



Figure 6: Error evolution comparison with  $m = 8000$ .Figure 7: Error evolution comparison with  $m = 80000$ .

We first validate that the error reduction by the gradient descent learning tends to the diffusion process (4.1) of the error  $\hat{\eta}_{NN}(\xi, \theta) = \hat{f}(\xi) - \widehat{\mathcal{N}}_s(\xi, \theta)$  in the Fourier spectral domain as the width of neural network goes to infinity. We take  $a = 4.2$ ,  $b = 5.8$  and the initial errors are given by  $\eta_{NN}(x, \theta_0) = \mathcal{N}_s(x, \theta_0) - f(x)$  with parameters initialized by sampling from independent random variables of normal distribution. In the gradient descent learning,

the training data set consists of 1000 uniformly distributed points in  $[-1,1]$  and learning rate  $\tau=1.0e-3$  is adopted. In the Fourier spectral domain, the diffusion equation (4.1) with initial function  $\hat{\eta}(\xi, \theta_0) = \widehat{\mathcal{N}}_s(\xi, \theta_0) - \hat{f}(\xi)$  are solved by using the Hermite spectral method introduced above. We take  $p=100$  and  $\Delta t = \tau$  in the discretization. Noting that [3,5]

$$\mathcal{F}^{-1}[\widehat{H}_k(\xi)](x) = \int_{-\infty}^{+\infty} \widehat{H}_k(\xi) e^{2i\pi\xi x} d\xi = \sqrt{2\pi} i^k \widehat{H}_k(2\pi\xi), \quad (4.27)$$

the  $p$ -th order Hermite spectral approximation

$$\hat{\eta}_p(\xi, \theta(t_m)) = \sum_{k=0}^p \hat{\eta}_k^m \widehat{H}_k(\lambda\xi), \quad (4.28)$$

can be analytically transformed back to physical domain as

$$\eta_p(x, \theta(t_m)) = \sum_{k=0}^p \hat{\eta}_k^m \int_{-\infty}^{+\infty} \widehat{H}_k(\lambda\xi) e^{2i\pi x \xi} d\xi = \frac{\sqrt{2\pi}}{\lambda} \sum_{k=0}^p \hat{\eta}_k^m i^k \widehat{H}_k\left(\frac{2\pi x}{\lambda}\right). \quad (4.29)$$

Then, the errors  $\eta_{NN}(x, \theta(t_m))$  and  $\eta_p(x, \theta(t_m))$  evolved by gradient descent method and diffusion equations are compared in Fig. 6-7. We provide numerical results for different width of neural network with  $m=8000, 80000$  while the number of scales is fixed to be  $s=3$ . Although the initial errors are different for neural networks with different number of neurons, the evolution of the error matches quite well.

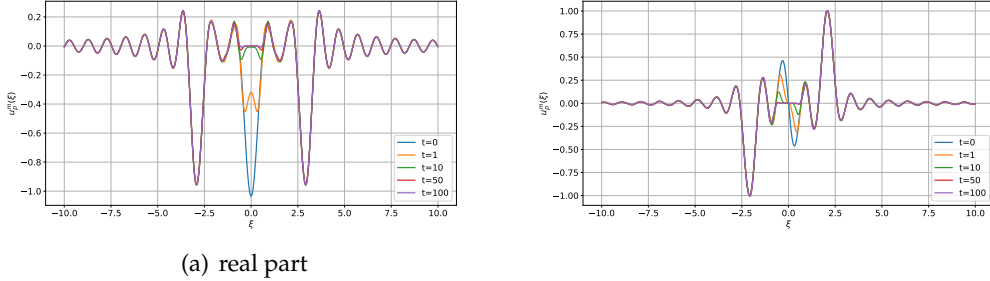
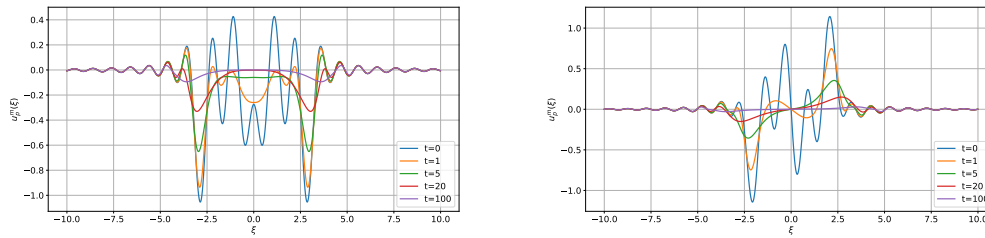


Figure 8: Numerical solution of (4.1) with coefficients  $\{A_0^\pm(\xi), B_0^\mp\}$ .

Now, we are able to use the numerical solution of the diffusion equation (4.1) to show the advantages of using multi-scale neural network. We set  $m=8000$ ,  $a=4.2$ ,  $b=5.8$  and the initial errors are given by  $\hat{\eta}(\xi, \theta_0) = \widehat{\mathcal{N}}_s(\xi, \theta_0) - \hat{f}(\xi)$  with parameters initialized by sampling from independent random variables of normal distribution. In the discretization of the diffusion equation (4.1), we take  $p=100$  and  $\Delta t = 1.0e-3$ . The numerical solution of the diffusion equations with coefficients  $\{A_0^\pm(\xi), B_0^\mp\}$  and  $\{A_3^\pm(\xi), B_3^\mp\}$  at different time  $t$  are plotted in Fig. 8-Fig. 9. We can see that diffusion coefficients  $\{A_0^\pm(\xi), B_0^\mp\}$  only produce decay in a very small neighborhood of the origin while the coefficients



(a) imaginary part

Figure 9: Numerical solution of (4.1) with coefficients  $\{A_3^\pm(\xi), B_3^\mp\}$ .

$\{A_3^\pm(\xi), B_3^\mp\}$  produce much faster decay in a large interval. Although the initial errors are different, the numerical results still verify that multi-scale neural networks has better performance than fully connected ones.

## 5 Conclusion and future work

In this paper, we investigated the convergence of the machine learning algorithm using multi-scale neural network by deriving diffusion models for the error of the MscaleDNN in either approximating oscillatory functions or solving BVP of ODEs. When the sine function is selected as the activation function, we show that the gradient descent learning leads to a diffusion process of the initial error in the Fourier frequency domain when the width of the neural network goes to infinity. At the same time, we show that the MscaleDNN with different scales leads to the same diffusion equation but with coefficients with wider support in the frequency domain. To study the quantitatively behavior of the diffusion models, a Hermite spectral method is employed to produce highly accurate numerical solutions for the diffusion equation. Numerical results show that the diffusion coefficients corresponding to the multi-scale neural network will generate faster decay speed and wider decay range on the initial function with the increasing of the number of the scales. This is consistent with the performance of the multi-scale neural network which has faster convergence especially in the approximation of highly oscillated functions. Moreover, we also numerically show that the derived diffusion equation can be used to predict the convergence of the machine learning algorithm even when the width of the neural network is not very large.

This work is just the beginning of the theoretical analysis for the multi-scale neural network, with many challenge problems in this direction. The analysis for the multi-scale deep neural network with other popular activation functions, e.g., ReLU, Sigmoid, etc, is the most import future work.

## Acknowledgments

B. W. Wang acknowledges the financial support provided by NSFC (grant 12022104), the Construct Program of the Key Discipline in Hunan Province. W. Z. Zhang acknowledges the financial support provided by NSFC (grant 12201603)

## References

- [1] I. Daubechies. *Ten lectures on wavelets*. SIAM, 1992.
- [2] W. E and B. Yu. The deep Ritz method: a deep learning-based numerical algorithm for solving variational problems. *Commun. Math. Stat.*, 6(1):1–12, 2018.
- [3] I. S. Gradshteyn and I. M. Ryzhik. *Table of integrals, series, and products*. Academic press, 2014.
- [4] A. Jacot, F. Gabriel, and C. Hongler. Neural tangent kernel: Convergence and generalization in neural networks. *Proc. Adv. Neural Inf. Process. Syst.*, 31, 2018.
- [5] H. Y. Li, R. Q. Liu, and L. L. Wang. Efficient hermite spectral-Galerkin methods for nonlocal diffusion equations in unbounded domains. *Numer. Math-Theory Me.*, 2022.
- [6] Y. J. Liu and C. Yang. Vpvnet: a velocity-pressure-vorticity neural network method for the stokes' equations under reduced regularity. *arXiv preprint arXiv:2112.07131*, 2021.
- [7] Z. Q. Liu, W. Cai, and John Z. Q. Xu. Multi-scale deep neural network (MscaleDNN) for solving poisson-boltzmann equation in complex domains. *Commun. Comput. Phys.*, 28(5):1970–2001, 2020.
- [8] Y. F. Peng, D. Hu, and John Z. Q. Xu. A non-gradient method for solving elliptic partial differential equations with deep neural networks. *J. Comput. Phys.*, 472:111690, 2023.
- [9] M. Raissi and G. E. Karniadakis. Hidden physics models: Machine learning of nonlinear partial differential equations. *J. Comput. Phys.*, 357:125–141, 2018.
- [10] M. Raissi, P. Perdikaris, and G. E. Karniadakis. Physics-informed neural networks: A deep learning framework for solving forward and inverse problems involving nonlinear partial differential equations. *J. Comput. Phys.*, 378:686–707, 2019.
- [11] J. Shen, T. Tang, and L.L. Wang. *Spectral Methods: Algorithms, Analysis and Applications*, volume 41 of *Springer Series in Computational Mathematics*. Springer-Verlag, Berlin, Heidelberg, 2011.
- [12] B. Wang, W. Z. Zhang, and W. Cai. Multi-scale deep neural network (MscaleDNN) methods for oscillatory stokes flows in complex domains. *Commun. Comput. Phys.*, 28(5):2139–2157, 2020.
- [13] John Z.Q. Xu, Y. Y. Zhang, T. Luo, Y. Y. Xiao, and Z. Ma. Frequency principle: Fourier analysis sheds light on deep neural networks. *Commun. Comput. Phys.*, 28(5):1746–1767, 2020.